Journal of Materials Chemistry

Cite this: J. Mater. Chem., 2012, 22, 25057

www.rsc.org/materials

PAPER

Influence of a novel fluorosurfactant modified PEDOT:PSS hole transport layer on the performance of inverted organic solar cells†

Fang Jeng Lim,[ab] Krishnamoorthy Ananthanarayanan,[b] Joachim Luther[bc] and Ghim Wei Ho*[a]

Received 20th August 2012, Accepted 1st October 2012
DOI: 10.1039/c2jm35646e

Under ambient conditions the long term stability of non-encapsulated organic solar cells with conventional device architecture is lower than the technical lifetime of devices with an inverted configuration. The removal of the interface between the ITO (indium tin oxide) layer and the acidic PEDOT:PSS layer along with the substitution of a low work function metal electrode with a high work function metal electrode in the inverted device configuration renders relatively higher stability in these devices. However, one of the main inherent difficulties involving the fabrication of devices with such inverted architecture is the wettability of the hydrophilic PEDOT:PSS onto the photoactive layer such as the P3HT:PCBM blend which is hydrophobic in nature. To overcome this, we have used a novel fluorosurfactant, Capstone® Dupont™ FS-31 (CFS-31), as a substitute to the conventional Zonyl FS-300 as an additive to PEDOT:PSS. A smooth and uniform PEDOT:PSS layer was coated onto the P3HT:PCBM blend layer by addition of CFS-31 alone without any further treatments. Using this surfactant, an efficiency of 3.1% and a stable device performance (up to 400 hours) under ambient conditions without encapsulation have been achieved.

1 Introduction

Though impressive progress with improving the power conversion efficiency of organic solar cells (OSCs) has been made, their practical use is still hampered due to their inherent poor stability.[1–4] The degradation of organic semiconductors in the presence of oxygen and moisture still remains a key issue that needs to be addressed by the research community.[5,6] Device instability of non-encapsulated conventional OSCs under ambient conditions is often ascribed to the etching of the indium-doped tin oxide (ITO) substrate by the acidic poly(3,4-ethylenedioxythiophene)–poly(styrenesulfonate) (PEDOT:PSS) and the presence of an easily oxidized low work function metal electrode like aluminium.[7] Inverted device architecture is frequently adopted to overcome the above stated disadvantages. In this type of architecture, PEDOT:PSS is shifted to the top of the photoactive layer instead of being in contact with the ITO (see Fig. 1(a) and (b) for device architecture comparison) and in addition to this a more air-stable high work function metal such as silver or gold is used as the metal electrode. Due to these

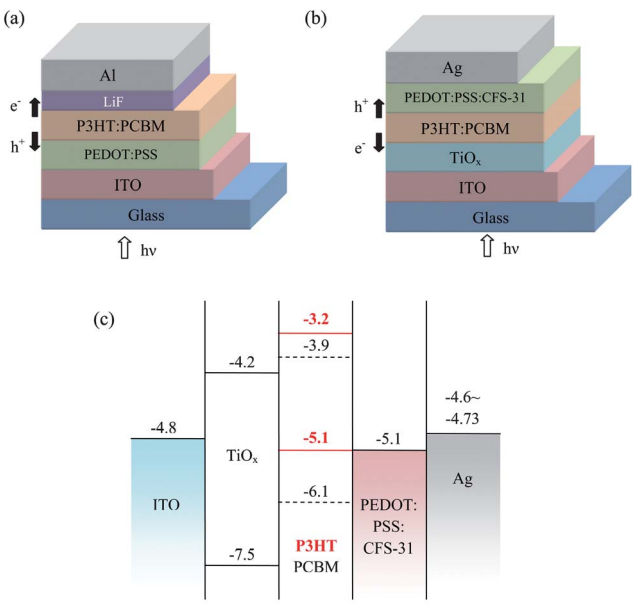

Fig. 1 (a) Typical non-inverted organic solar cell device architecture and (b) inverted organic solar cell device architecture ITO/TiO_x/P3HT:PCBM/PEDOT:CFS-31/Ag; (c) energy level diagram of an inverted organic solar cell. The energy values are in eV with respect to the vacuum level. The red lines and black dashed lines correspond to the HOMO and LUMO of P3HT and PCBM, respectively. The respective energy levels were obtained from ref. 29–31.

[a]*Department of Electrical and Computer Engineering, National University of Singapore, Blk EA #06-10, 9 Engineering Drive 1, 117575 Singapore. E-mail: elehgw@nus.edu.sg; Fax: +65 6775 4710; Tel: +65 6516 8121*
[b]*Solar Energy Research Institute of Singapore (SERIS), National University of Singapore, 7 Engineering Drive 1, 117574 Singapore*
[c]*Department of Material Science and Engineering, National University of Singapore, Blk E4 #01-01, 9 Engineering Drive 1, 119260 Singapore*
† Electronic supplementary information (ESI) available. See DOI: 10.1039/c2jm35646e

advantages, a device with inverted architecture is expected to show better stability under ambient conditions compared to its non-inverted conventional counterpart.

OSCs with inverted architecture require selective electron transporting layers (ETLs) and hole transporting layers (HTLs) for effective charge transport. N-type metal oxides such as TiO_x,[8–10] ZnO[11–13] and Cs_2CO_3[14–16] were generally used as an ETL. This layer is also necessary to break the symmetry of the charge carrier pathways. Consequently, ITO becomes the electron collecting electrode and the metal becomes the hole collecting electrode. Materials such as MoO_x[15,17] and PEDOT:PSS[9,11] were normally used as a HTL. Many research groups have indeed shown that the inverted OSCs have longer device stability than conventional devices.[18–20] Yang *et al.* have recently reported an inverted bulk heterojunction (BHJ) device based on the PBDTTT-C-T/$PC_{71}BM$ blend with gold nanoparticles and nanograting design with an efficiency of 8.79% (device stability was not reported and the device efficiency was not certified independently).[21] Hau *et al.* demonstrated an inverted flexible OPV device using ZnO as an interfacial layer which could retain 80% of the initial device performance after 40 days of exposure in air.[18] McGehee *et al.* reported a PCDTBT polymer based OSC with inverted architecture that shows a shelf life of 7 years under encapsulation under ambient conditions.[22]

Though encouraging device performance (with respect to both stability and efficiency) is seen in inverted OPV devices, coating of PEDOT:PSS onto the photoactive layer remains to be one of the main technical challenges involved in the fabrication of these devices. The hydrophobic nature of the underlying photoactive layer (such as P3HT:PCBM) produces high surface tension upon contact with hydrophilic PEDOT:PSS, causing a serious wettability issue. Without the aid of additives, PEDOT:PSS can hardly be coated onto the photoactive layer. Removal of PEDOT:PSS as a hole transport layer (HTL) is not an option to resolve this issue as this will render the photoactive layer susceptible to oxygen and moisture, causing detrimental effects on the device performance. Furthermore, the absence of a selective hole transport layer (HTL) would result in poor device performance.[23] Therefore, the use of additives is necessary to circumvent this wettability issue. Isopropyl alcohol (IPA) is the most commonly used additive for PEDOT:PSS to reduce the surface energy.[2] Other alternatives such as Triton X-100[24] and Zonyl FS-300[25] were also used previously. The use of fluorosurfactants such as Zonyl FS-300 is more beneficial than hydrocarbon based surfactants (Triton X-100) in reducing the surface tension between the PEDOT:PSS and the polymeric layer. This is attributed to the lipophobic nature of the C–F tail which tends to concentrate at a liquid–air interface, in contrast with the lipophilic C–H tail that concentrates in condensed phase interfaces.[26] In the fabrication of inverted OPV devices, Zonyl FS-300 is often used together with IPA because Zonyl FS-300 or IPA alone is insufficient for PEDOT:PSS to lie within the wetting envelope of P3HT:PCBM. Undesirable and detrimental surface treatment of the photoactive layer with UV-ozone prior to PEDOT:PSS coating is often required to increase its surface energy.[27]

In this work, we propose the use of a new type of non-ionic fluorosurfactant: Capstone® Dupont™ FS-31 (herein referred to as CFS-31) as a substitute to Zonyl FS-300 in the fabrication of an inverted OPV device. To the best of our knowledge, usage of CFS-31 in enhancing the wettability and film quality of PEDOT:PSS on top of the photoactive layer in inverted OPV devices has not been reported to date. CFS-31 is capable of providing remarkably low surface tension ($\sim$15 mN m^{-1}) compared to Zonyl FS-300 ($\sim$23 mN m^{-1}) in aqueous or solvent-based products (ideal for PEDOT:PSS) that could enable better wetting. We have conducted our studies with the bulk heterojunction P3HT:PCBM model system in inverted device architecture with solution-processed TiO_x as an electron transport layer (ETL) along with a PEDOT:PSS HTL with CFS-31 additive. The following positive aspects of CFS-31 are highlighted in this work: (1) improvement of the device performance of solution-processed TiO_x inverted OPV devices; (2) enabling of appropriate PEDOT:PSS coating onto P3HT:PCBM without requiring additional additives and surface treatments; (3) provision of the invariant optimal thickness of a TiO_x ETL; and (4) realization of a stable device performance for at least 400 hours when exposed to ambient atmosphere without encapsulation.

2 Experimental

2.1 Materials

Titanium isopropoxide (TTIP, 97%, Sigma Aldrich), acetylacetone (AA, Sigma Aldrich) and isopropanol (IPA, reagent grade, Aik Moh Paints & Chemical Pte Ltd.) were used to prepare the TiO_x electron transport layer. Regioregular (>98%) poly(3-hexylthiophene) (P3HT, product code M101, average M_w 65 500, Ossila), phenyl-C_{61}-butyric acid methyl ester ($PC_{61}BM$ – 99.5% purity, product code Nano-CPCBM-BF, Nano-C) and poly(3,4-ethylenedioxythiophene):poly(styrene sulfonate) (PEDOT:PSS – Heraeus Clevios P VP Al 4083, product code M121, Ossila) were used as donor, acceptor and hole transport layer, respectively. *ortho*-Dichlorobenzene (ODCB, Sigma Aldrich) was used as the solvent for the donor and acceptor. Capstone® FS-31 (Dupont) was added into PEDOT:PSS prior to spin coating. Silver (Ag) was purchased from K. J. Kurt Lesker & Co. All the above mentioned materials were used as received.

2.2 Solution preparation

The TiO_x precursor solution was prepared by adding an appropriate amount of acetylacetone dropwise into TTIP under continuous stirring. Isopropanol was then added into the mixture as a solvent. The volume ratio of TTIP : AA : IPA was set to 1 : 0.5 : 5. The sol was then stirred for at least 2 hours prior to spin coating onto the substrate. The as-prepared sol exhibited an orange-yellow color, indicating the d–d absorption originated from the titanium complex ion formed by the reaction between titanium isopropoxide and the stabilizer acetylacetone.[28] PEDOT:PSS/fluorosurfactant solution was prepared by blending the PEDOT:PSS solution with Capstone® FS-31 (CFS-31) with a 0 to 15% volume ratio with respect to PEDOT:PSS. The P3HT:PCBM blend was made in the ratio 1 : 0.8 (the concentration of P3HT was 15 mg ml^{-1}, whereas the PCBM concentration was found to give best results at 12 mg ml^{-1}) in 1 ml of ODCB. The mixed solution was stirred and heated at 60 °C overnight in a N_2 filled glove box prior to spin coating.

2.3 Device fabrication

Inverted bulk heterojunction organic solar cells based on P3HT:PCBM were prepared on pre-patterned indium tin oxide (ITO, Xinyan Technology Ltd.) coated glass substrates. The sheet resistance of the ITO (thickness: 90 ± 10 nm) was found to be around 15–20 Ω $\square^{-1}$. The substrates were pre-cleaned using a detergent solution, followed by successive sonication in de-ionized water, isopropanol and acetone for 15 minutes each. The substrates were then dried in an oven at 60 °C for two hours. Firstly, the prepared TiO_x sol was spin cast onto the substrate, followed by hydrolysis in air under a controlled condition of RH 45 ± 2%, 22 °C. The hydrolyzed films were then annealed at 180 °C (at a ramp rate of 1 °C min^{-1}). The annealed films were then transferred into the N_2 filled glove box without further treatment and spin coated with the P3HT:PCBM blend at 800 rpm for 30 seconds and the resultant wet film was then annealed on a hot plate at 140 °C for 1 minute. The thickness of the photoactive layer was found to be around 200 nm. 70 nm of PEDOT:PSS blended with various concentrations of CFS-31 (denoted as PEDOT:CFS-31 in future occurrences) was then coated onto the active layer in air through a 0.45 μm cellulose filter and annealed at 140 °C for 1 minute in the N_2 filled glove box. To complete the device, an Ag metal electrode (thickness: 100 nm) was then thermally evaporated through a shadow mask, resulting in an active device with an area of 9 mm^2. Each ITO-coated glass substrate contained 6 such devices. The vacuum during the evaporation was around 2×10^{-6} mbar. The finished device is of the architecture glass/ITO/TiO_x/P3HT:PCBM/PEDOT:CFS-31/Ag. Fig. 1(b) and (c) show the inverted OPV device architecture and the energy level diagram under flat band conditions. The energy levels for P3HT:PCBM, Ag and other layers were obtained from ref. 29–31, respectively. Cell degradation studies were carried out by storing the device under ambient atmosphere, following the ISOS-D shelf scheme.[32]

2.4 Instrumentation

The current density–voltage (j–V) measurements were carried out under 1 sun illumination (ABET technologies Sun 2000 solar simulator) whose intensity was calibrated using a calibrated silicon reference cell (Fraunhofer ISE). Steady-state j–V characteristics were recorded with a Keithley 2400 sourcemeter. The external quantum efficiency (EQE) of the solar cells was measured using a system developed by Bentham Instruments Ltd. The required illumination light was obtained using a light source (Xenon/halogen) which is coupled to a monochromator (TMc300 monochromator). To detect and measure small signals accurately, a lock-in amplifier along with a built-in chopper controller was used. A calibrated Si diode with known spectral response was used as a reference. Optical microscopy images of PEDOT:CFS-31 were taken using an optical microscope (Olympus BX 51M). Atomic force microscopy (AFM) images were taken using a Dimension 3100 atomic force microscope (Digital Instruments). The thicknesses of all the layers were measured using a Veeco DEKTAK 150 Stylus Profilometer. All the fabrication steps, except coating of TiO_x and PEDOT:PSS, were performed inside a glove box of N_2 atmosphere (Charslton Technologies, ≤1 ppm moisture and O_2).

3 Results and discussion

3.1 Effect of the fluorosurfactant concentration on device performance

Table 1 and Fig. 2 show the device performance of inverted BHJ solar cells with PEDOT:PSS HTL and TiO_x ETL as a function of varying concentration of CFS-31. The data were collected and averaged (for at least 10 reproducible cells). As can be seen from Fig. 2, a concentration region of 4–8% CFS-31 in PEDOT:PSS is required for high device performance. The amount of CFS-31 required to achieve an optimal device performance can be controlled with relative ease. When the surfactant concentration is low (0–4%), high surface tension between the hydrophilic PEDOT:PSS and the hydrophobic P3HT:PCBM results in non-wetting and non-uniform films. The large amount of surface defects that are present between the two layers inherently cause high leakage current and high series resistance, resulting in a low fill factor and consequently poor device efficiency. In this regime (0–4%), the device is characterized by no or poor coverage of the HTL on P3HT:PCBM. The absence of hole selectivity between the P3HT:PCBM–Ag interface increases the interfacial recombination losses significantly. As the surfactant concentration increases towards 4%, a more uniform layer of PEDOT:PSS starts to form which results in a well defined hole extraction layer. This well defined layer results in an increase in the open circuit voltage (V_{oc}), short circuit current density (j_{sc}) and fill factor (FF).

In the optimal surfactant concentration region (4–8%), the champion device had an efficiency of 3.1% which is higher than that of the previously reported solution processed TiO_x ETL inverted OPV devices (P3HT:PCBM as a photoactive layer) using various other additives.[9,28,33] The enhanced device efficiency compared to devices with low surfactant concentration (less than 4%) is attributed to a less significant hindrance of the PEDOT conductive pathway imposed by the CFS-31 molecules.

Table 1 Photovoltaic parameters of the P3HT:PCBM inverted organic solar cells studied under different conditions (j_{sc}: short circuit current density, V_{oc}: open circuit voltage, and FF: fill factor). Device structure for the inverted organic solar cells: glass/ITO/TiO_x/P3HT:PCBM/PEDOT:PSS-CFS-31/Ag. The active area of all cells is 0.09 cm^2. The thickness of TiO_x is about 130–140 nm. The error values given in the square brackets correspond to the maximum standard deviation of the device characteristic parameters over at least 10 reproducible cells

PEDOT:CFS-31 volume ratio [%]	V_{oc} [±20 mV]	j_{sc} [±0.6 mA cm^{-2}]	FF [±6%]	Efficiency [±0.3%]
0.0	318	5.2	32.5	0.5
0.5	308	4.8	27.8	0.4
1.0	503	5.2	35.9	0.9
1.5	623	7.2	44.1	2.0
2.0	600	7.8	49.5	2.3
3.0	600	7.4	54.9	2.4
3.5	607	7.8	54.9	2.6
4.0	594	8.0	63.6	3.0
4.5	605	8.2	62.6	3.1
5.0	613	8.0	63.0	3.1
5.5	607	7.8	65.4	3.1
6.0	612	7.6	65.0	3.0
8.0	599	7.8	65.4	3.1
10.0	603	7.2	61.3	2.7
15.0	593	6.2	59.2	2.2

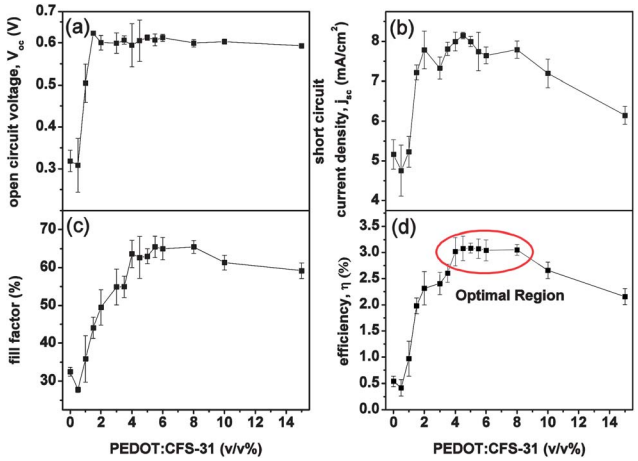

Fig. 2 Device performance showing (a) V_{oc}, (b) j_{sc}, (c) fill factor and (d) efficiency values of inverted OSCs with various PEDOT:CFS-31 concentration ratios (volume ratio ranging from 0 to 15 vol%). The error bars represent the standard deviation of the device characteristics over at least 10 reproducible cells. The device active area is 0.09 cm^2. The thickness of TiO_x is about 130–140 nm.

This will consequently form films with low defect density and high uniformity, giving a high fill factor of 66% that is close to the predicted maximum for P3HT:PCBM based devices.[34] Relatively good charge carrier transfer and extraction with minimal bimolecular and interfacial recombination is observed within this concentration regime, resulting in a high j_{sc}. Furthermore, V_{oc} is very close to the effective bandgap of P3HT and PCBM, suggesting a good ohmic contact throughout the device.[35] In the case of a high surfactant concentration (>8%), j_{sc} becomes the detrimental factor for the observed reduced device performance (Fig. 2). This observation is attributed to the hindrance in the hole conduction pathway of PEDOT by the surfactant molecules as confirmed by the microscopic image in Fig. 4. This phenomenon was also observed earlier when PEDOT:PSS is added with excess Zonyl FS-300 surfactant.[36]

The variation in the observed fill factor in the range of surfactant concentrations used in this study follows from the corresponding j–V characteristics and resistances of representative samples under illumination as shown in Fig. 3(a) and (b). Since the resistivity in OPV devices is voltage and area dependent, the shunt resistance (R_{sh}) was extracted by averaging dV/dI around zero bias ($V = 0$) conditions whereas the series resistance (r_s) was extracted around V_{oc} of the respective device. A large gradient (dV/dI) at $V = 0$ (large R_{sh}) is desired as this indicates less defective interfaces. On the other hand, a low gradient (dV/dI) at $V = V_{oc}$ (low r_s) is desired as this translates to good lateral connection within the same layers for better charge

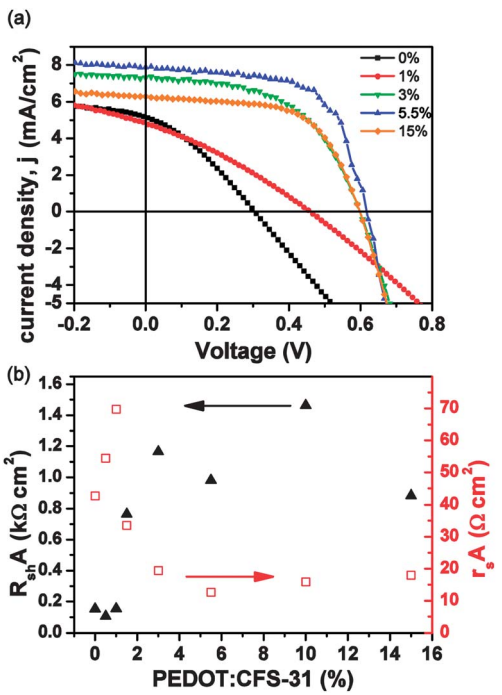

Fig. 3 (a) Illuminated j–V characteristics of representative devices with different CFS-31 surfactant concentrations, (b) shunt (▲) and series (□) resistances of the corresponding device extracted from (a). The device active area is 0.09 cm^2.

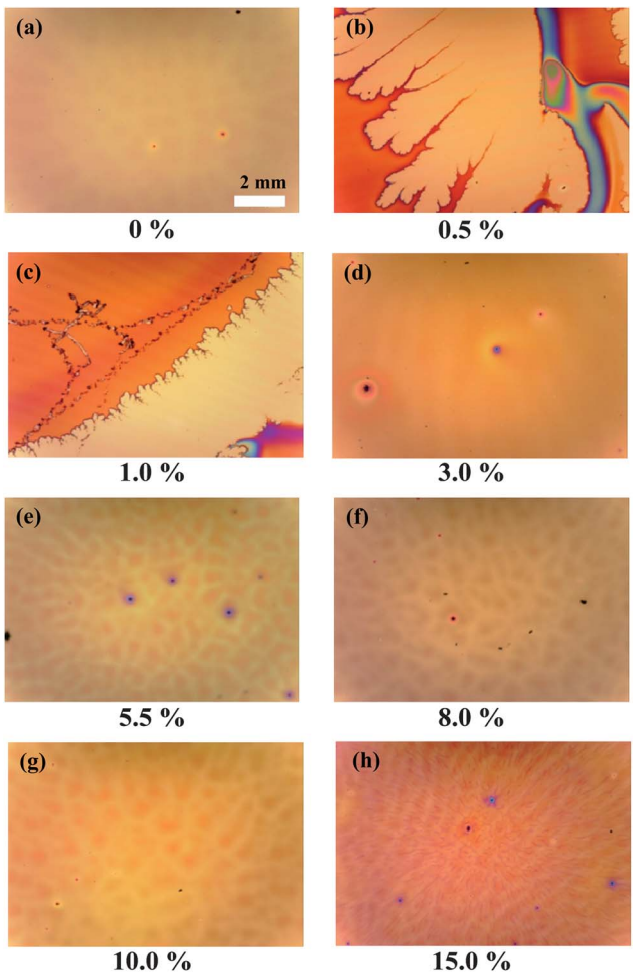

Fig. 4 Optical microscopy images under 5× magnification showing P3HT:PCBM/PEDOT:CFS-31 with (a) 0%, (b) 0.5%, (c) 1.0%, (d) 3.0%, (e) 5.5%, (f) 8.0%, (g) 10.0%, and (h) 15.0%. In (a)–(d), dark orange region – PEDOT:PSS, yellow region – P3HT:PCBM; in (e)–(g), bright (yellow) networks – PEDOT, dark (orange) regions – PSS clusters; (h) pink networks indicating phase segregation.

extraction. In the absence of a surfactant, almost no PEDOT:PSS was coated on P3HT:PCBM (see Fig. 4(a)). We observed a large leakage current ($R_{sh}A = 0.15$ kΩ cm^2) and large series resistance ($r_sA = 42.8$ Ω cm^2) (the active area of the device is 0.09 cm^2). A thick and non-uniform PEDOT:PSS layer was formed in the low surfactant concentration regime (0.5–1%). This has direct influence on the series resistance of the device. As evidenced in Fig. 3(b), we observe an increase in the series resistance of the device in this regime and also a large leakage current (low shunt resistance, $R_{sh}A = 0.11$ kΩ cm^2). This is due to the high defect density present in the film. Furthermore, the inferior PEDOT:PSS film formation on P3HT:PCBM caused by poor adhesion is a problematic issue for lateral conduction ($r_sA = 54.5$ Ω cm^2). When the surfactant concentration increases beyond 1.0%, a sharp increase in the shunt resistance and a decrease in series resistance were observed. The PEDOT:PSS film slowly becomes more uniform and less defective as the surfactant concentration increases, giving rise to high shunt resistance which stabilizes at around 1–1.4 kΩ cm^2. Correspondingly, the series resistance decreases from 69.8 Ω cm^2 to 12.6 Ω cm^2. The series resistance indeed increases slowly when the concentration of the surfactant increases beyond 5.5% and this leads to a slight decrease in the fill factor of the device. However, the cause for the reduced device performance is still attributed predominantly to the reduction in j_{sc}. For the purpose of further device analysis, samples with 5.5% CFS-31 were chosen. The corresponding champion device performance is as follows: $V_{oc} = 607$ mV, $j_{sc} = 7.8$ mA cm^{-2}, fill factor (FF) = 65% and efficiency = 3.1%.

Fig. 5 shows the external quantum efficiency (EQE) of devices with 0% and 5.5% surfactant concentrations. EQEs of around 25% and 53% were observed, respectively. A low device EQE can be attributed to combinatorial effects of relatively poor light absorption, charge separation and charge carrier extraction (effect of charge transport, contacts and recombination). Since there is no appreciable difference in the UV-vis absorption spectra and photoluminescence for these two devices formed under identical conditions (see Fig. S1 and S2 in the ESI†), we can assume that both devices share the same charge generation and separation. Hence, poor charge carrier extraction in the 0% surfactant device is possibly a key reason for the lower EQE. Since poor device charge carrier extraction is often caused by various loss mechanisms such as bi-molecular recombination, charge trapping and trap-assisted recombination,[37–39] a correspondingly lower j_{sc} (and thus lower efficiency) is expected.

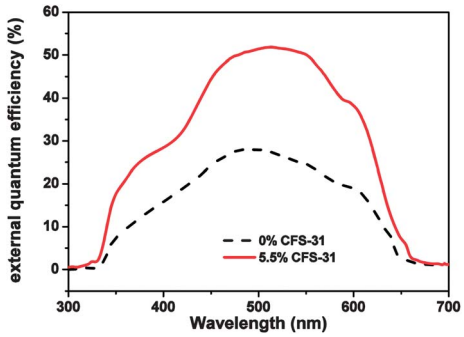

Fig. 5 External quantum efficiency (EQE) of a device with 0% (black dotted line) and 5.5% (red solid line) CFS-31 concentrations.

3.2 Effect of the surfactant concentration on film morphology

Fig. 4(a)–(h) show the optical microscopy images taken with 5× magnification of PEDOT:CFS-31 on the P3HT:PCBM film. The morphology observed shows strong correlation with the device performance. When no CFS-31 is added (Fig. 4(a)), the high surface tension prevents PEDOT:PSS from adhering onto P3HT:PCBM, giving a high contact angle and hence resulting in almost no PEDOT:PSS layer coated. As a result, only the P3HT:PCBM layer is observed. At low surfactant concentrations ranging from 0.5 to 1% (Fig. 4(b) and (c)), poor coverage of PEDOT:PSS onto P3HT:PCBM is observed. The observed morphology strongly correlates with the corresponding poor performance of the device as discussed previously (Fig. 2). Once a layer of the PEDOT:PSS film is able to fully cover the P3HT:PCBM layer (observed from 1.5% CFS-31 onwards, the representative image is shown in Fig. 4(d)), the device V_{oc} increases to 600 mV and remains constant with further increase of the surfactant concentration. However, the PEDOT:PSS at this stage is still not yet well phase-separated. The phase separation of PEDOT and PSS chains is crucial for PEDOT to form a conductive channel which enhances the charge carrier transport.[36]

In the optimal region (5.5% surfactant concentration, Fig. 4(e)), films with bright (yellow) networks and dark (orange) regions were observed. We attribute the bright networks and dark clusters to the PEDOT networks and PSS agglomerates, respectively. Based on AFM imaging studies, it is known that PEDOT tends to form three-dimensional networks and PSS tends to form agglomerates.[40,41] Bao *et al.* have recently reported that the addition of a moderate amount of non-ionic fluorosurfactant such as Zonyl FS-300 promotes phase segregation of PEDOT and PSS.[36] Thus, by correlating this image with the device performance, we can infer that CFS-31 also promotes PEDOT:PSS phase segregation which results in the formation of a well defined PEDOT conduction pathway and also helps in maintaining a good contact with the P3HT:PCBM photoactive layer. The low root-mean-square roughness (3.2 nm) shown in the corresponding atomic force microscopy (AFM) height image in Fig. 6 further reaffirms the existence of a good contact between PEDOT:PSS and P3HT:PCBM.

Further increase in the concentration (Fig. 4(f)–(h)) will further promote phase segregation while having conduction pathways blocked by the surfactant molecules. The blocking effect is especially evident in the sample with 15% surfactant concentration (Fig. 4(h)) by the formation of pink networks on the PEDOT:PSS film. As seen from the optical microscopy image, an increase of the surfactant concentration eventually results in a hindrance of the PEDOT:PSS network by the surfactant molecule. It is also reported earlier that excess Zonyl FS-300 will cause a detrimental effect on the film morphology.[36] Therefore, we conclude that any further addition of CFS-31 will cause a detrimental effect on the device performance and indeed we are able to correlate this with the observation of a significant decrease in the short circuit current density of the device in Fig. 2(b).

In addition, we would like to emphasize that by using CFS-31 alone, the PEDOT:PSS lies within the wetting envelope of P3HT:PCBM (minimum wetting surface tension,

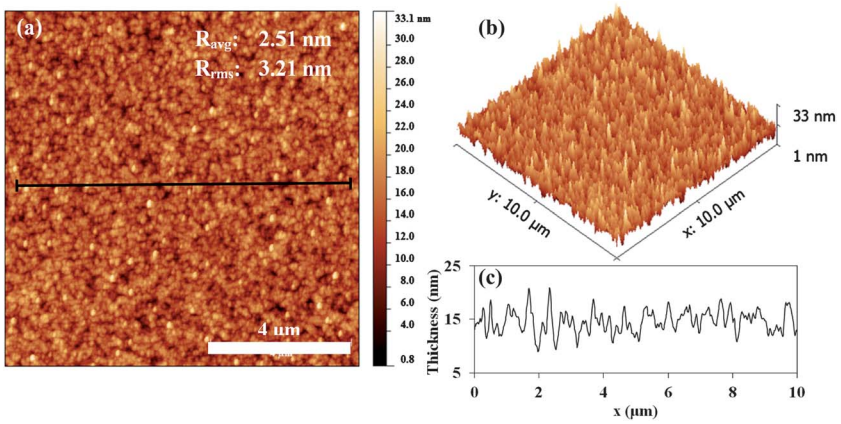

Fig. 6 Atomic force microscopy (AFM) images showing a (a) 2D topographical image, (b) 3D topographical image and (c) 2D surface profile. The profile corresponds to the black line indicated in (a). 5.5% CFS-31 concentration was used during the fabrication of the cells.

$\gamma \sim 28$ mN m^{-1}) without requiring additives such as IPA.[27,42] It is also worth mentioning here that there is no need for further surface treatment with UV ozone to reduce the surface energy of P3HT:PCBM. The oxygen surface treatment is known to have unfavorable effects on the device performance by forming oxygen induced traps.[43]

3.3 Effect of TiO_x thickness

The presence of a selective electron transport layer (ETL) in inverted OPV devices is as important as the selective hole transport layer. We have conducted a systematic study on the variation of the thickness of the TiO_x ETL layer on the device performance using a device fabricated with a 5.5% CFS-31 concentration. The variation in the TiO_x thickness was achieved by varying the spin coating speed of the precursor solution. Fig. 7 shows V_{oc}, j_{sc}, fill factor and efficiency with varying TiO_x thicknesses. The device shows optimal performance in the thickness range (TiO_x) of 130–140 nm. In the absence of TiO_x, the absence of the hole blocking effect results in a high amount of interfacial recombination, giving rise to poor selective charge extraction to the ITO.[23] This effect is strongly reflected in the low V_{oc} and j_{sc} observed in the device. At an optimal thickness of 130 nm, TiO_x not only effectively performs the role of an ETL but also acts as a protective layer for the donor–acceptor blend from the attack of superoxides or hydrogen peroxide caused by UV light.[9] The superoxides and hydrogen peroxides from air and moisture aggressively attack the adjoining P3HT:PCBM layer and lower the device stability.[32] The TiO_x layer prepared in this study is amorphous in nature as the annealing temperature used is only 180 °C. As a consequence, a large amount of sub-band trap states are formed. Above the optimal thickness, these impurities slightly absorb visible light and hence lower the overall amount of light absorbed by the photoactive P3HT:PCBM layer.[9] TiO_x at its optimal thickness is able to provide the optimal UV filtering effect without significantly decreasing visible light absorption of P3HT:PCBM. It yields the best result with a device efficiency of 3.1%. CFS-31 added PEDOT:PSS devices provide better device performance compared to IPA added (2.06%) and Zonyl FS-300 added (2.61%) devices at a TiO_x thickness of ~100 nm[9] and ~50 nm,[33] respectively.

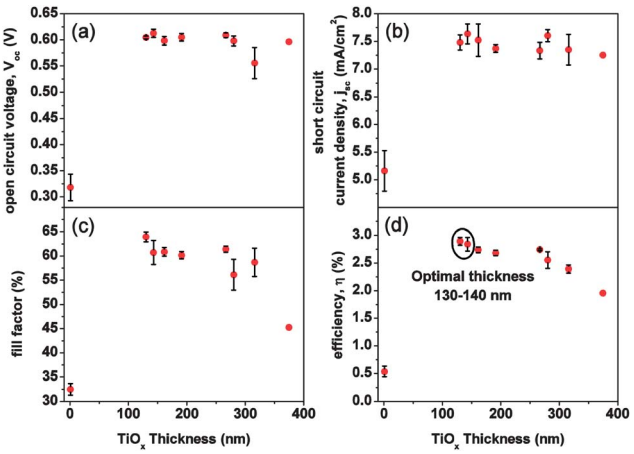

Fig. 7 Device performance showing (a) V_{oc}, (b) j_{sc}, (c) fill factor and (d) efficiency values of a 5.5% CFS-31 concentration inverted OPV device with TiO_x thickness ranging from 0 to 380 nm. The error bars represent the standard deviation of the device characteristic parameters over at least 10 reproducible cells. The device active area is 0.09 cm^2.

3.4 Degradation study

The addition of this novel surfactant into PEDOT:PSS shows no detrimental effects on the stability of the inverted device under ambient conditions (Fig. 8). We can observe that the device has superior stability over non-encapsulated non-inverted devices, which degraded to 50% of its initial value in less than 3 hours after exposure to air (Fig. 8, inset). The inverted devices were light-soaked for approximately 10 to 20 minutes before recording the parameters to fill the trap states of TiO_x.[28,29] A sample with an optimized concentration of CFS-31 (5.5%) is able to retain almost 76% of its initial device performance even after 400 hours when exposed to ambient air (without encapsulation). This reveals that Capstone® FS-31 has no detrimental effects on the photoactive layer, P3HT:PCBM. The observed degradation of the device efficiency is mainly caused by the continual decrease in j_{sc}. This is attributed to the change in both chemical and physical morphologies of the active layer components of the device.[43]

During the initial exposure in air, the device efficiency increases by up to 25% compared to freshly prepared cells. We

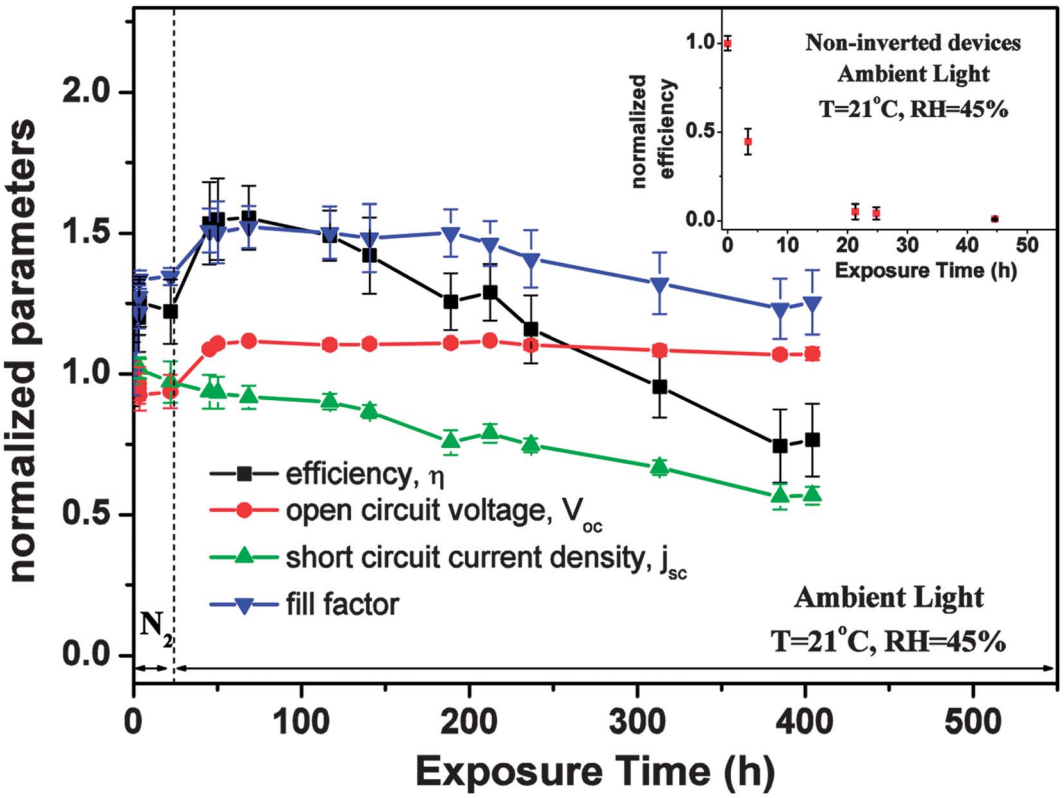

Fig. 8 Device performance showing normalized open circuit voltage, short circuit current density, fill factor and efficiency of a 5.5% CFS-31 concentration inverted OPV device under exposure in a N_2 (left of the dashed vertical line) and in an ambient atmosphere (right of the dashed vertical line) without encapsulation. The parameters were normalized by their respective initial values. The ambient atmosphere refers to relative humidity = 45% and temperature = 21 °C. Inset: normalized efficiency of non-inverted devices under ambient air exposure conditions without encapsulation.

have also observed an initial increase in the V_{oc} and fill factor but a decrease of j_{sc} with time. Lloyd *et al.* also observed a similar phenomenon without using PEDOT:PSS.[19] The initial increase in the efficiency for the as-fabricated device stored under ambient conditions is attributed to the oxidation of silver to silver oxides. This results in a shift of the work function to −5.0 eV with respect to the vacuum level, which in turn increases the V_{oc}.[19,30] Detailed studies are required to further understand the mechanism. Nevertheless, we can conclude that addition of CFS-31 to PEDOT:PSS improves the wettability without having any detrimental effects on the photoactive layer.

4 Conclusions

A systematic study on the role of a new type of fluorosurfactant Capstone® Dupont™ FS-31 (CFS-31) as a substitute for conventional surfactants in inverted organic solar cells was carried out. Smooth and uniform films that lie within the wetting envelope of P3HT:PCBM can be achieved by CFS-31 alone without the need of additional additives and/or UV ozone treatment on P3HT:PCBM. Optimal device parameters such as TiO_x thickness did not alter compared to samples prepared without using CFS-31. Addition of CFS-31 to PEDOT:PSS is not detrimental for hole transport from P3HT to the Ag contact. We have demonstrated that solution processed TiO_x inverted OPV cells using CFS-31 added PEDOT:PSS exhibit a device efficiency of up to 3.1%. At least 65% of the initial performance was retained in the course of 400 hours for the optimized device without encapsulation. All these attributes of CFS-31 make it more advantageous than standard surfactants. Capstone® Dupont™ FS-31 seems to be beneficial for overcoming wettability issues encountered in the fabrication of solution-processed inverted organic photovoltaic devices.

Acknowledgements

SERIS is sponsored by the National University of Singapore (NUS) and Singapore's National Research Foundation (NRF) through the Singapore Economic Development Board (EDB). Fang Jeng Lim would also like to express his sincere gratitude to NRF (Energy Innovation Programme Office) for providing a PhD scholarship. We gratefully acknowledge Dupont™ through MegaChem Limited, Singapore for supplying Capstone® FS-31.

References

1 W. Cai, X. Gong and Y. Cao, Polymer solar cells: recent development and possible routes for improvement in the performance, *Sol. Energy Mater. Sol. Cells*, 2010, **94**(2), 114–127.
2 T. Stubhan, H. Oh, L. Pinna, J. Krantz, I. Litzov and C. J. Brabec, Inverted organic solar cells using a solution processed aluminum-doped zinc oxide buffer layer, *Org. Electron.*, 2011, **12**(9), 1539–1543.
3 M. Jørgensen, K. Norrman, S. Gevorgyan, T. Tromholt, B. Andreasen and F. Krebs, Stability of polymer solar cells, *Adv. Mater.*, 2012, **24**(5), 580–612.
4 H. Yip and A. Jen, Recent advances in solution-processed interfacial materials for efficient and stable polymer solar cells, *Energy Environ. Sci.*, 2012, **5**(3), 5994–6011.

5 E. Katz, S. Gevorgyan, M. Orynbayev and F. Krebs, Out-door testing and long-term stability of plastic solar cells, *Eur. Phys. J.: Appl. Phys.*, 2006, **36**(3), 307.
6 N. Espinosa, R. García-Valverde, A. Urbina, F. Lenzmann, M. Manceau, D. Angmo and F. C. Krebs, Life cycle assessment of ITO-free flexible polymer solar cells prepared by roll-to-roll coating and printing, *Sol. Energy Mater. Sol. Cells*, 2012, **97**, 3–13.
7 H. Kim, S. Nam, H. Lee, S. Woo, C. Ha, M. Ree and Y. Kim, Influence of controlled acidity of hole-collecting buffer layers on the performance and lifetime of polymer: fullerene solar cells, *J. Phys. Chem. C*, 2011, **115**(27), 13502–13510.
8 T. Kuwabara, H. Sugiyama, M. Kuzuba, T. Yamaguchi and K. Takahashi, Inverted bulk-heterojunction organic solar cell using chemical bath deposited titanium oxide as electron collection layer, *Org. Electron.*, 2010, **11**(6), 1136–1140.
9 H. Sun, J. Weickert, H. C. Hesse and L. Schmidt-Mende, UV light protection through TiO_2 blocking layers for inverted organic solar cells, *Phys. Chem. Chem. Phys.*, 2011, **95**(12), 3450–3454.
10 C. Waldauf, M. Morana, P. Denk, P. Schilinsky, K. Coakley, S. Choulis and C. Brabec, Highly efficient inverted organic photovoltaics using solution based titanium oxide as electron selective contact, *Appl. Phys. Lett.*, 2006, **89**, 233517.
11 Z. Liang, Q. Zhang, O. Wiranwetchayan, J. Xi, Z. Yang, K. Park, C. Li and G. Cao, Effects of the morphology of a ZnO buffer layer on the photovoltaic performance of inverted polymer solar cells, *Adv. Funct. Mater.*, 2012, **22**(10), 2194–2201.
12 M. S. White, D. C. Olson, S. E. Shaheen, N. Kopidakis and D. S. Ginley, Inverted bulk-heterojunction organic photovoltaic device using a solution-derived ZnO underlayer, *Appl. Phys. Lett.*, 2006, **89**(14), 143517.
13 C. Zhang, H. You, Z. Lin and Y. Hao, Inverted organic photovoltaic cells with solution-processed zinc oxide as electron collecting layer, *Jpn. J. Appl. Phys.*, 2011, **50**(8), 082302.
14 G. Li, C. W. Chu, V. Shrotriya, J. Huang and Y. Yang, Efficient inverted polymer solar cells, *Appl. Phys. Lett.*, 2006, **88**(25), 253503.
15 Y. Lee, J. Youn, M. Ryu, J. Kim, H. Moon and J. Jang, Electrical properties of inverted poly(3-hexylthiophene): methano-fullerene [6,6]-phenyl-C_{71}-butyric acid methyl ester bulk hetero-junction solar cell with Cs_2CO_3 and MoO_3 layers, *Sol. Energy Mater. Sol. Cells*, 2011, **95**(12), 3276–3280.
16 H. H. Liao, L. M. Chen, Z. Xu, G. Li and Y. Yang, Highly efficient inverted polymer solarcell by low temperature annealing of Cs_2CO_3 interlayer, *Appl. Phys. Lett.*, 2008, **92**(17), 173303.
17 X. W. Sun, D. W. Zhao, L. Ke, A. K. K. Kyaw, G. Q. Lo and D. L. Kwong, Inverted tandem organic solar cells with a MoO_3/Ag/Al/Ca intermediate layer, *Appl. Phys. Lett.*, 2010, **97**(5), 053303.
18 S. K. Hau, H. L. Yip, N. S. Baek, J. Zou, K. O'Malley and A. K. Y. Jen, Air-stable inverted flexible polymer solar cells using zinc oxide nanoparticles as an electron selective layer, *Appl. Phys. Lett.*, 2008, **92**(25), 253301–253303.
19 M. T. Lloyd, D. C. Olson, P. Lu, E. Fang, D. L. Moore, M. S. White, M. O. Reese, D. S. Ginley and J. W. P. Hsu, Impact of contact evolution on the shelf life of organic solar cells, *Phys. Chem. Chem. Phys.*, 2009, **19**(41), 7638–7642.
20 T. Y. Chu, S. W. Tsang, J. Zhou, P. G. Verly, J. Lu, S. Beaupré, M. Leclerc and Y. Tao, High-efficiency inverted solar cells based on a low bandgap polymer with excellent air stability, *Sol. Energy Mater. Sol. Cells*, 2012, **96**, 155–159.
21 X. Li, W. C. H. Choy, L. Huo, F. Xie, W. E. I. Sha, B. Ding, X. Guo, Y. Li, J. Hou, J. You and Y. Yang, Dual plasmonic nanostructures for high performance inverted organic solar cells, *Adv. Mater.*, 2012, **24**(22), 3046–3052.
22 C. Peters, I. Sachs-Quitana, J. Kastrop, S. Beaupré, M. Leclerc and M. McGehee, High efficiency polymer solar cells with long operating lifetimes, *Adv. Energy Mater.*, 2011, **1**(4), 491–494.
23 J. Servaites, M. Ratner and T. Marks, Organic solar cells: a new look at traditional models, *Energy Environ. Sci.*, 2011, **4**(11), 4410–4422.
24 W. Baek, M. Choi, T. Yoon, H. Lee and Y. Kim, Use of fluorine-doped tin oxide instead of indium tin oxide in highly efficient air-fabricated inverted polymer solar cells, *Appl. Phys. Lett.*, 2010, **96**, 133506.
25 D. J. Lipomi, B. C. K. Tee, M. Vosgueritchian and Z. Bao, Stretchable organic solar cells, *Adv. Mater.*, 2011, **23**(15), 1771–1775.
26 Mason Chemical Company, *Fluorosurfactant – Structure and Function*, http://www.masonsurfactants.com/Products/Fluorosurfactant.htm, 2007, [5/19/2012].
27 M. M. Voigt, R. C. Mackenzie, C. P. Yau, P. Atienzar, J. Dane, P. E. Keivanidis, D. D. Bradley and J. Nelson, Gravure printing for three subsequent solar cell layers of inverted structures on flexible substrates, *Sol. Energy Mater. Sol. Cells*, 2011, **95**(2), 731–734.
28 T. Kuwabara, T. Nakayama, K. Uozumi, T. Yamaguchi and K. Takahashi, Highly durable inverted-type organic solar cell using amorphous titanium oxide as electron collection electrode inserted between ITO and organic layer, *Sol. Energy Mater. Sol. Cells*, 2008, **92**(11), 1476–1482.
29 T. Kuwabara, C. Iwata, T. Yamaguchi and K. Takahashi, Mechanistic insights into UV-induced electron transfer from PCBM to titanium oxide in inverted-type organic thin film solar cells using AC impedance spectroscopy, *ACS Appl. Mater. Interfaces*, 2010, **2**(8), 2254–2260.
30 J. Kim, C. Kim, Y. Kim and Y. Loo, Oxidation of silver electrodes induces transition from conventional to inverted photovoltaic characteristics in polymer solar cells, *Appl. Phys. Lett.*, 2009, **95**, 183301.
31 C. J. Brabec, V. Dyakonov, and U. Scherf, Organic Photovoltaics: Materials, *Device Physics, and Manufacturing Technologies*, Wiley-VCH, 2008, p. 575.
32 M. Reese, S. Gevorgyan, M. Jørgensen, E. Bundgaard, S. Kurtz, D. Ginley, D. Olson, M. Lloyd, P. Morvillo and E. Katz, Consensus stability testing protocols for organic photovoltaic materials and devices, *Sol. Energy Mater. Sol. Cells*, 2011, **95**(5), 1253–1267.
33 M. Bolognesi, A. Sánchez-Díaz, J. Ajuria, R. Pacios and E. Palomares, The effect of selective contact electrodes on the interfacial charge recombination kinetics and device efficiency of organic polymer solar cells, *Phys. Chem. Chem. Phys.*, 2011, **13**(13), 6105–6109.
34 R. Mauer, I. Howard and F. Laquai, Effect of nongeminate recombination on fill factor in polythiophene/methanofullerene organic solar cells, *J. Phys. Chem. Lett.*, 2010, **1**(24), 3500–3505.
35 F. Zhang, X. Xu, W. Tang, J. Zhang, Z. Zhuo, J. Wang, J. Wang, Z. Xu and Y. Wang, Recent development of the inverted configuration organic solar cells, *Sol. Energy Mater. Sol. Cells*, 2011, **95**(7), 1785–1799.
36 M. Vosgueritchian, D. J. Lipomi and Z. Bao, Highly conductive and transparent PEDOT:PSS films with a fluorosurfactant for stretchable and flexible transparent electrodes, *Adv. Funct. Mater.*, 2012, **22**(2), 421–428.
37 R. C. I. MacKenzie, T. Kirchartz, G. F. A. Dibb and J. Nelson, Modeling nongeminate recombination in P3HT:PCBM solar cells, *J. Phys. Chem. C*, 2011, **115**(19), 9806–9813.
38 L. Tzabari and N. Tessler, Shockley-Read-Hall recombination in P3HT:PCBM solar cells as observed under ultralow light intensities, *J. Appl. Phys.*, 2011, **109**, 064501.
39 M. Kuik, H. Nicolai, M. Lenes, G. Wetzelaer, M. Lu and P. Blom, Determination of the trap-assisted recombination strength in polymer light emitting diodes, *Appl. Phys. Lett.*, 2011, **98**, 093301.
40 X. Crispin, F. L. E. Jakobsson, A. Crispin, P. C. M. Grim, P. Andersson, A. Volodin, C. V. Haesendonck, M. V. D. Auweraer, W. R. Salaneck and M. Berggren, The origin of the high conductivity of poly(3,4-ethylenedioxythiophene)−poly-(styrenesulfonate) (PEDOT−PSS) plastic electrodes, *Chem. Mater.*, 2006, **18**(18), 4354–4360.
41 Y. Xia and J. Ouyang, PEDOT:PSS films with significantly enhanced conductivities induced by preferential solvation with cosolvents and their application in polymer photovoltaic cells, *J. Mater. Chem.*, 2011, **21**(13), 4927–4936.
42 D. Kwok and A. Neumann, Contact angle measurement and contact angle interpretation, *Adv. Colloid Interface Sci.*, 1999, **81**(3), 167–249.
43 N. Grossiord, J. M. Kroon, R. Andriessen and P. W. Blom, Degradation mechanisms in organic photovoltaic devices, *Org. Electron.*, 2012, **13**(3), 432–456.

